

Passing gas through the hydrate stability zone at southern Hydrate Ridge, offshore Oregon

Xiaoli Liu ^{*}, Peter B. Flemings

Department of Geosciences, The Pennsylvania State University, University Park, PA, 16802, USA

Received 4 March 2005; received in revised form 3 August 2005; accepted 21 October 2005

Available online 28 November 2005

Editor: E. Boyle

Abstract

We present an equilibrium model of methane venting through the hydrate stability zone at southern Hydrate Ridge, offshore Oregon. Free gas supplied from below forms hydrate, depletes water, and elevates salinity until pore water is too saline for further hydrate formation. This system self-generates local three-phase equilibrium and allows free gas migration to the seafloor. Log and core data from Ocean Drilling Program (ODP) Site 1249 show that from the seafloor to 50 m below seafloor (mbsf), pore water salinity is elevated to the point where liquid water, hydrate and free gas coexist. The elevated pore water salinity provides a mechanism for vertical migration of free gas through the regional hydrate stability zone (RHSZ). This process may drive gas venting through hydrate stability zones around the world. Significant amount of gaseous methane can bypass the RHSZ by shifting local thermodynamic conditions.

© 2005 Elsevier B.V. All rights reserved.

Keywords: Gas hydrate; Hydrate ridge; Free gas migration; Salinity

1. Introduction

Gas hydrate is an ice-like compound that contains methane and/or other low molecular weight gas in the lattice of water molecules [1]. Although most of the seafloor lies within the low-temperature and high-pressure conditions necessary for hydrate formation, hydrate is generally found in sediments along continental margins [2], where adequate supplies of gas are available [3]. The large volumes of gas stored in hydrate are a potential energy resource [4]. Release of large volumes of methane from hydrate into the ocean and atmosphere may play a role in the past climate change [5]. Pressure

increase due to rapid hydrate decomposition may contribute to failure along continental margins where gas hydrate is found [6].

Southern Hydrate Ridge lies at ~800 m water depth in the Cascadia accretionary complex (Fig. 1). A bottom-simulating reflector (BSR) is imaged pervasively beneath it [7]. The BSR is a strong, negative-polarity, strata-crossing, seismic reflector that mimics the seabed and records the phase boundary between gas hydrate above and free gas below [8,9]. Gas vents, hydrate outcrops, authigenic carbonate deposits, and chemosynthetic organisms are present on the seafloor [10,11]. A 50-m-high pinnacle of authigenic carbonate is located ~350 m southwest of the summit [12]. Beneath the Pinnacle, there is a zone of low reflectivity (wipeout) overlying a weak and disrupted BSR (Fig. 2).

^{*} Corresponding author. Tel.: +1 814 863 9663; fax: +1 814 863 7823.

E-mail address: xliu@geosc.psu.edu (X. Liu).

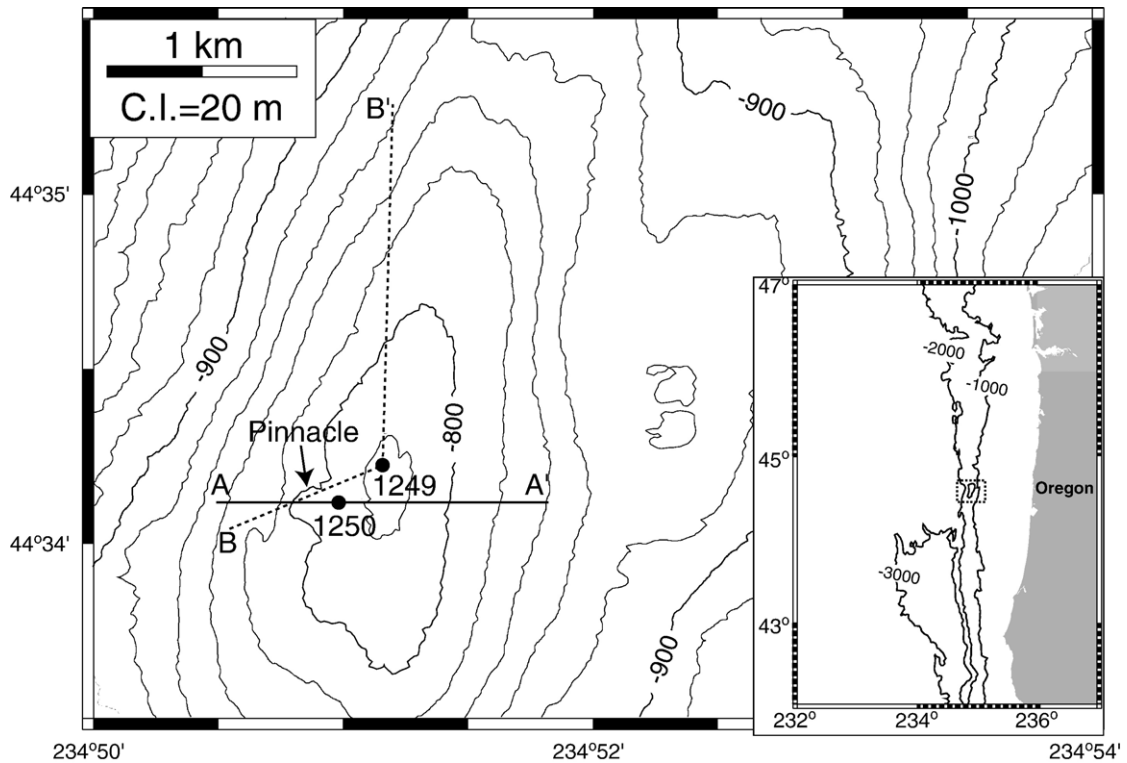


Fig. 1. Topography of southern Hydrate Ridge (in meters below sea level). Contour interval is 20 m. Inset map shows location of Hydrate Ridge. Bathymetric contour interval is 1000 m.

Hydrate stability depends on pressure, temperature, the gas concentration in the surrounding pore water, and the activity of water [1] (Fig. 3). Liquid (subscript

L) and gas (subscript G) coexist below the three-phase equilibrium curve, while liquid and hydrate (subscript H) coexist above it (Fig. 3C). We define the regional

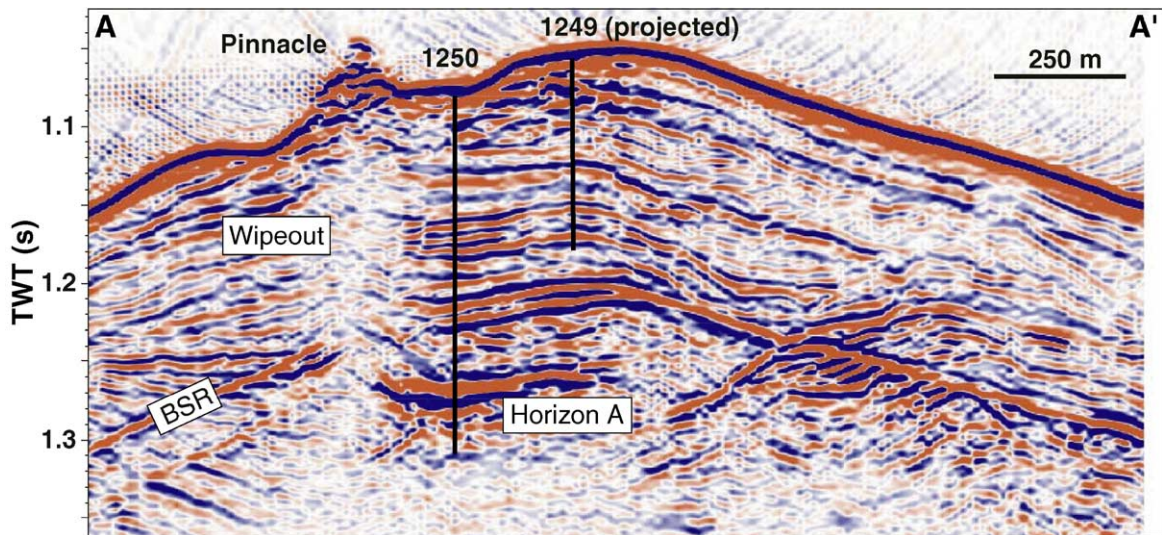


Fig. 2. Seismic cross section through the summit (A–A' in Fig. 1, modified from Trehu et al. [12]). The bottom-simulating reflector (BSR) is a negative-polarity reflection that marks the phase boundary between gas hydrate above and free gas below. A bright, negative polarity reflection (Horizon A) stretches laterally beneath the BSR. High free gas saturations are present over some distance within Horizon A [40]. The BSR is disrupted where Horizon A crosses the RHSZ but is continuous elsewhere. A low-amplitude chimney is present above the disrupted BSR and is

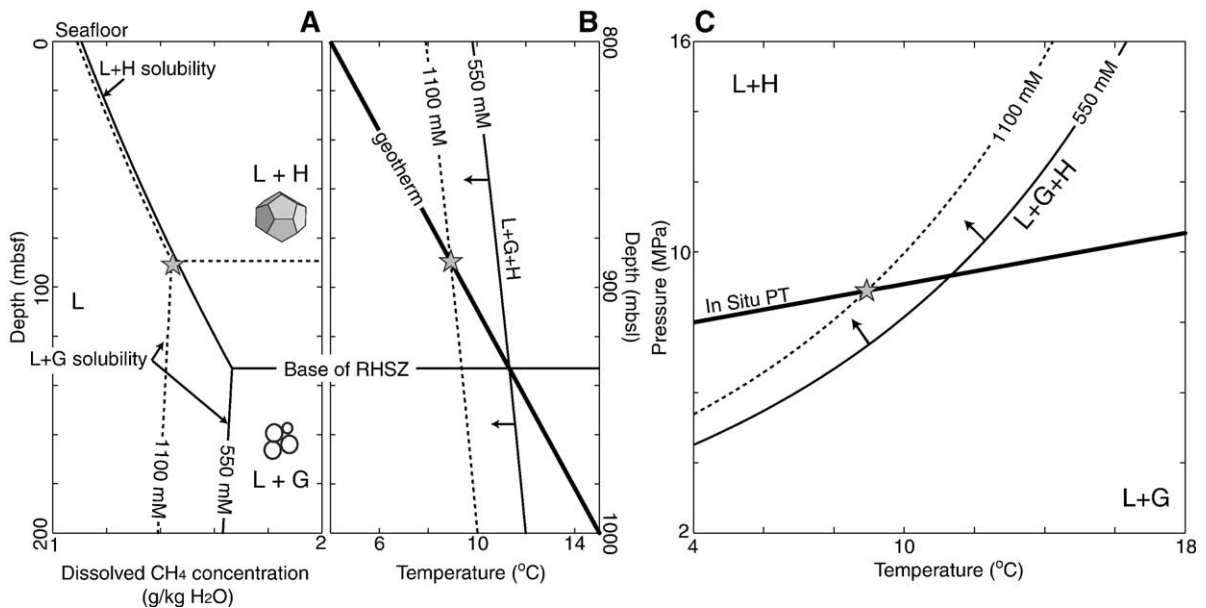


Fig. 3. (A) CH₄ solubility, (B) temperature for three-phase equilibrium and (C) hydrate stability P - T phase diagram for salinities of 550 (solid line) and 1100 mM Cl⁻ (dotted line). Fields of hydrate (H), dissolved (L) and free gas (G) are depicted. (A) Hydrate or free gas is present only when the gas concentration exceeds the solubility. The peak in solubility coincides with the base of the RHSZ for seawater salinity (550 mM Cl⁻). (B) The intersection of the geotherm with the temperature for three-phase equilibrium defines the base of the RHSZ. (C) Solid arrows indicate the displacement of the phase boundary when salinity increases. At southern Hydrate Ridge, water depth is ~800 m, pressure gradient is hydrostatic (~10 MPa/km), seafloor temperature is 4 °C and geothermal gradient is 55 °C/km [14]. mbsf—meters below sea floor; mbsl—meters below sea level.

hydrate stability zone (RHSZ) as the zone where hydrate is stable for seawater salinity (550 mM Cl⁻). At southern Hydrate Ridge, the base of the RHSZ is predicted to be ~130 m below seafloor (mbsf) (Fig. 3B). Water coexists with hydrate inside the RHSZ, whereas water and free gas are stable below the RHSZ. In this stratified gas hydrate system, the zone of three-phase equilibrium corresponds to a single depth (~130 mbsf) and free gas should not be present within the RHSZ.

However, there is abundant evidence that free gas exists and migrates inside the RHSZ at southern Hydrate Ridge. Venting of methane bubbles at the seafloor indicates rapid passage of methane-rich fluids through the RHSZ [10]. X-ray computer tomography (CT) studies on near-surface samples record gas within hydrate layers [13]. Hydrate samples collected near the seafloor have a gas bubble texture [11]. At ODP (Ocean Drilling Program) Site 1249, a PCS (Pressure Core Sampler) measurement (~14 mbsf) records the presence of in situ free gas [14]. A Fugro pressure core (~14 mbsf) from a different hole was logged in the storage chamber, and showed an interval with a very low bulk density (~0.75 g/cm³) [12].

Three mechanisms are envisaged for eruption of free gas through the RHSZ. First, gas flow may be out of equilibrium with its surroundings due to kinetic effects [15,16]. Second, hydrate formation may be limited by the availability of water when gas is supplied in excess of its proportion in hydrate [17,18]. Third, the P - T boundary defining the RHSZ may be perturbed upward by advecting warm fluids [19], capillary effects in fine-grained sediments [18,20], or high pore water salinity [14–16].

We build upon recent suggestions [14–16] that hyper-saline pore water shifts the three-phase stability boundary to allow free gas migration through the RHSZ. We present an equilibrium model to describe how the three-phase zone extends to the seafloor throughout the RHSZ and permits methane gas to escape into the ocean. We predict the evolution and distribution of salinity and gas hydrate along the gas migration path. The measured pore water salinities at Site 1249 are corrected to the in situ conditions; the corrected salinities in the upper ~50 mbsf agree well with model predictions, indicating that free gas and hydrate coexist in situ. We propose that hydrate formation is a self-equilibrating process in marine environments where a large volume of free gas is transported into the RHSZ.

2. Development of an equilibrium model for hydrate formation

2.1. Thermodynamic conditions for hydrate stability

The distribution of hydrate and free gas in the sediment column depends on two P – T dependent equilibrium solubility curves (Fig. 3A): (1) the liquid–hydrate (L+H) methane solubility curve where gas hydrate is at equilibrium with dissolved gas in water, and free gas is absent; and (2) the liquid–gas (L+G) methane solubility curve where free gas is at equilibrium with dissolved gas in water, and hydrate is absent. The model by Duan et al. [21] is used to predict the L+G equilibrium. The model by Henry et al. [20] is used to predict the L+H equilibrium. Comparison of model predictions with the CSMHYD hydrate program [1] shows good agreement.

The L+H solubility increases downward from the seafloor, while the L+G solubility slightly increases upward to the seafloor. At their intersection, three-phase equilibrium is present and CH_4 solubility reaches a maximum (Fig. 3A). The base of the RHSZ is located at the three-phase equilibrium for CH_4 +seawater salinity. When dissolved CH_4 concentration exceeds the solubility, hydrate is stable within the RHSZ while free gas is stable below the RHSZ.

Doubling pore water salinity from 550 to 1100 mM Cl^- reduces the L+G solubility by 15%, while the L+H solubility is relatively insensitive to the salinity increase (Fig. 3A). As a result, the intersection of the two solubility curves shifts upward from 130 to 90 mbsf. Accordingly, the base of the hydrate stability zone shifts from 130 to 90 mbsf (Fig. 3B). Elevated pore water salinity decreases hydrate stability conditions (Fig. 3C).

2.2. Hydrate formation and salinity increase in a box model

We explore how salinity change that occurs during hydrate formation affects hydrate stability. A sediment volume within the RHSZ is initially saturated with seawater (550 mM Cl^-) and local thermodynamic equilibrium is assumed. P – T conditions are assumed constant (volume expansion and latent heat of hydrate formation are ignored). Free methane gas is supplied to the sediment volume from below. This system is analogous to natural systems where abundant gas is supplied to sediment of low permeability.

Hydrate, like water ice, excludes dissolved salt during its formation, which increases the salinity of the

surrounding pore water [22]. Assuming there is no hydrate originally and all of the salts remain dissolved in water, the mass conservation of salts yields the relation between the pore water salinity (C), the initial salinity (C_i) and the hydrate saturation (S_h):

$$C = \frac{C_i}{1 - S_h}. \quad (1)$$

Note that the total volume actually expands under continuous supply of methane and constant P – T condition [23,24]. S_h in Eq. (1) represents the hydrate fraction in the original volume, if the volume change of hydrate formation is neglected. When free gas becomes stable, it expands the total volume without changing the hydrate fraction in the original space.

With addition of methane, the system evolves from a single phase (L) to two phases (L+H), to three phases (L+H+G) (Fig. 4). Initially all the methane is dissolved in water (L) and hydrate is absent. As methane is added, the methane concentration increases until it reaches the L+H solubility limit whereupon hydrate forms. Thereafter, the amount of methane in solution is limited by the solubility (Fig. 4D) and additional methane is transferred to the growing hydrate phase (Fig. 4A). During the L+H stage, the liquid is progressively enriched in salt with continued hydrate formation as illustrated in Eq. (1) (Fig. 4B). The L+H solubility decreases slightly while the L+G solubility decreases significantly (Fig. 4D). The increase in salinity causes an increase in the fugacity of methane in the liquid phase ($f_L^{\text{CH}_4}$) (Fig. 4C).

Once the fugacity of methane in solution ($f_L^{\text{CH}_4}$) equals that of gaseous methane ($f_G^{\text{CH}_4}$) (Fig. 4C), three-phase equilibrium between hydrate, salt solution and free gas is achieved. The L+G and L+H methane solubilities are the same at three-phase equilibrium (Fig. 4D). At this critical state, there is no further hydrate formation and any additional methane is present in the gas phase.

2.3. Hydrate formation by upward migration of free gas in a sediment column

We next describe how hydrate saturation and salinity evolve in a sediment column that is initially filled with seawater (Fig. 5). Free gas is supplied from below the RHSZ. We assume vertical gas flow, local thermodynamic equilibrium, that there is no water flux, and that there is no large-scale diffusion. Volume change and latent heat of hydrate formation are not considered; thus the temperature gradient is assumed constant and the pressure profile is assumed hydrostatic.

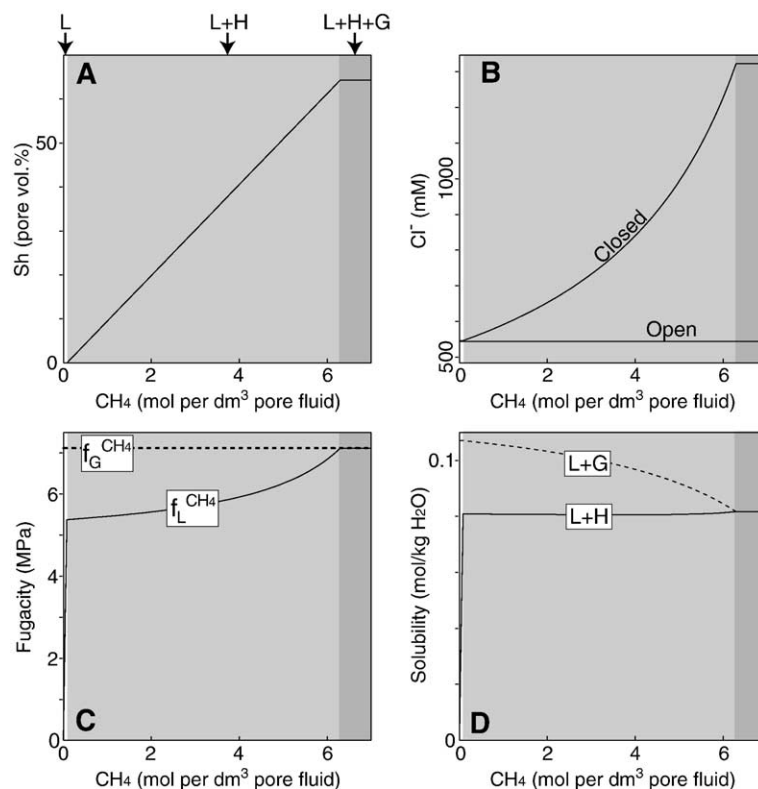


Fig. 4. Changes in (A) hydrate saturation, (B) salinity, (C) dissolved CH₄ fugacity and (D) concentration as CH₄ is added (in mol per dm³ of pore fluids) to a sediment volume at 50 mbsf ($P=8.5$ MPa, $T=6.75$ °C) from southern Hydrate Ridge. Single-phase (L), two-phase (L+H) and three-phase (L+G+H) fields are indicated by white, gray and dark areas respectively. Dashed lines in (C) and (D) indicate the fugacity and concentration of dissolved CH₄ that would be in equilibrium with free gas if hydrate did not form.

Initially, gas enters the base of the RHSZ and becomes hydrated. As hydrate forms, pore water salinity increases until free gas can coexist with hydrate (Fig. 5, Time 1). At this point, gas migrates further upward and hydrate forms at successively shallower depths (Fig. 5, Time 2). A sharp front in hydrate saturation and salinity is present at the top of the gas invasion zone and moves upward with time. Ultimately, the three-phase zone expands to the seafloor (Fig. 5, Time 3). At this point, there is a steady gas flow from below the RHSZ to the seafloor, the system is everywhere in three-phase equilibrium, and gas is vented into the ocean.

This process of hydrate formation is termed a flow-controlled front reaction [25]. Hydrate is formed as an advancing reaction front that separates the three-phase stability region behind from the unaltered region ahead. Behind the front, the water available for hydrate formation is not completely depleted, but the high salinity of the residual water prevents its reaction with gas to form more hydrate at the ambient P – T conditions. Hydrate formation only occurs at the reaction front

where both water and gas (i.e., reactants) are available. Ultimately, the reaction front propagates to the seafloor. In this model hydrate formation is essentially limited by the availability of pure water.

The salinity necessary for three-phase equilibrium increases upward toward the seafloor (Fig. 5). Near the base of the RHSZ, the P – T conditions are close to the expected three-phase boundary for seawater salinity. Thus only a small amount of hydrate forms before salinity builds enough to achieve three-phase equilibrium. In contrast, the P – T conditions at the seafloor are furthest away from the expected three-phase boundary for seawater salinity. The salinity required for three-phase equilibrium is not achieved until hydrate saturation increases to ~70%.

When the three-phase zone reaches the seafloor, there is a steady state (Fig. 5, Time 3). At this point, methane released at the seafloor equals that delivered at the base of the RHSZ and no more hydrate accumulates. The steady-state hydrate saturation and salinity profiles are independent of the gas supply rate and depend only on pressure and temperature. The gas

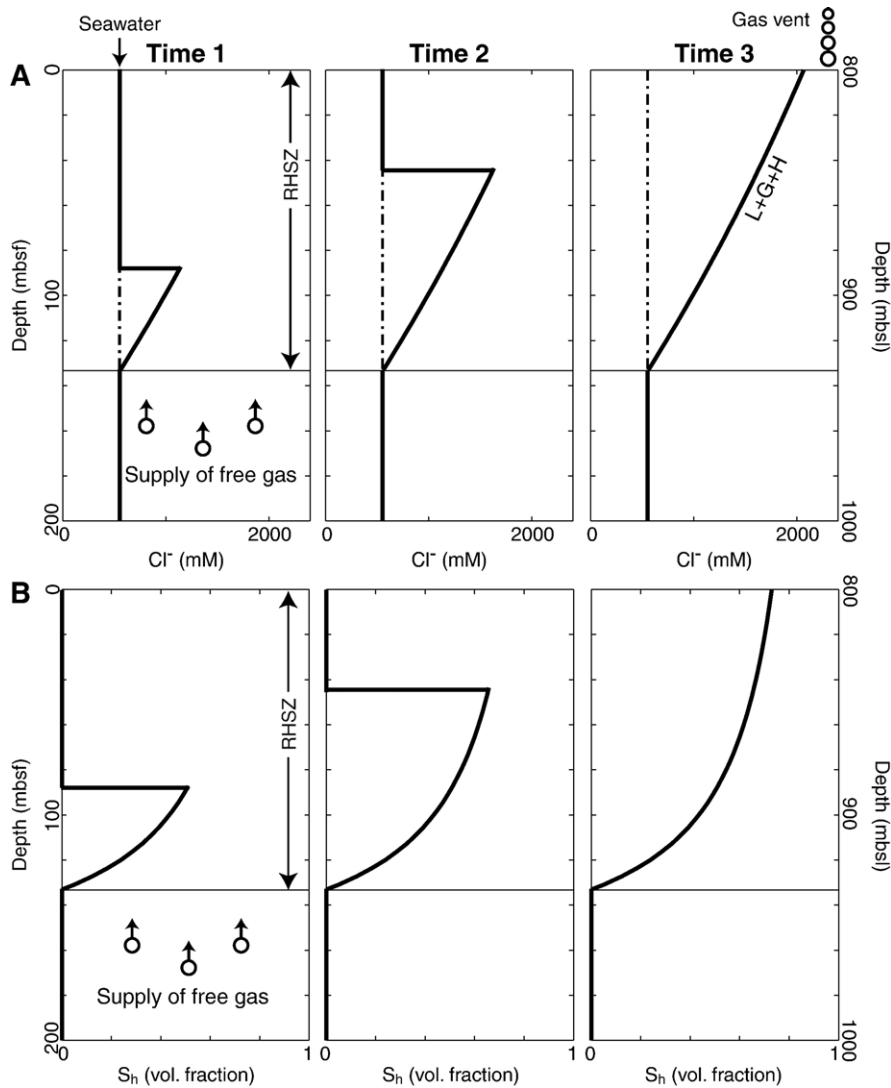


Fig. 5. Evolution of (A) salinity and (B) hydrate saturation in a sediment column due to the sustained gas flux from below. Initially, free gas migrates upward into the RHSZ and becomes hydrated at the base. Salinity increases due to the exclusion of salt from hydrate. Gas migrates upward further once the salinity is elevated to the point where three phases coexist. The salinity front grows with time from the base of the RHSZ towards the seafloor. A steady state profile eventually develops when the gas invasion zone reaches the seafloor and a gas vent is formed.

flux does control the rate at which the three-phase zone propagates to the seafloor.

We can test the assumption of local equilibrium through calculating the equilibration length (l_e) [25], which is

$$l_e = \frac{u_g}{\gamma}, \quad (2)$$

where u_g is the gas Darcy velocity and γ is the reaction rate constant. l_e is the characteristic distance in the flow direction over which free gas remains out of equilibrium with its surroundings. If l_e is much smaller than the model dimensions, nonequilibrium effects are negli-

ble. Experiments on hydrate formation suggest that $\gamma \approx 10^{-3} \text{ s}^{-1}$ [26] and the distance between the BSR and the seafloor is on the order of 100 m. Under these conditions, the Darcy velocity must be much less than 0.1 m s^{-1} for local equilibrium to be present.

We have also assumed no large-scale diffusion. In fact, there is a vertical zone of elevated salinity through which gas is being transported within the RHSZ. Lateral diffusion of Cl^- will occur from this saline gas chimney to the bounding normal salinity pore water. Loss of salt through lateral diffusion would shift the thermodynamic equilibrium, allow more hydrate formation [15], and deplete upward gas flow. If vertical gas

supply far exceeds gas depletion caused by lateral diffusion of salt (Appendix), then hydrate formation will rapidly propagate upward and the lateral diffusion of salt from the sides of gas chimney can be neglected. Thus when gas flux is high, the inherently two-dimensional problem of gas chimney can be approximated by the one-dimensional model. In contrast, if lateral diffusion of salt outpaces gas supply from below, then three-phase equilibrium cannot be sustained. As a result, the chimney will be restricted to the lower part of the RHSZ and free gas will not reach the seafloor.

3. Application to southern Hydrate Ridge

3.1. ODP Site 1249

ODP Site 1249 was drilled on the summit of southern Hydrate Ridge to a depth of 90 mbsf (Fig. 2). The

BSR at this site is at ~115 mbsf. Sediments are mainly composed of clay and silty clay [12] and the permeability measured at Site 1244 is low, ranging from 1.5×10^{-16} to 3×10^{-17} m² [27].

Log and core data from Site 1249 suggest that massive hydrate lenses extend to 30 mbsf near the summit of southern Hydrate Ridge (Fig. 6). The caliper log indicates an oversized borehole that may be associated with dissociated hydrate in the upper 10 mbsf (Fig. 6B). Between 10 and 20 mbsf, several massive gas hydrate layers have high resistivities (20 to 100 Ω m) and low formation densities (as low as 1.1 g/cm³). Pressurized cores recovered from 8 and 14 mbsf indicate hydrate pore volume saturations of ~45% [28]. Negative thermal anomalies, probably caused by adiabatic gas expansion and/or endothermic hydrate dissociation, are commonly measured (Fig. 6C).

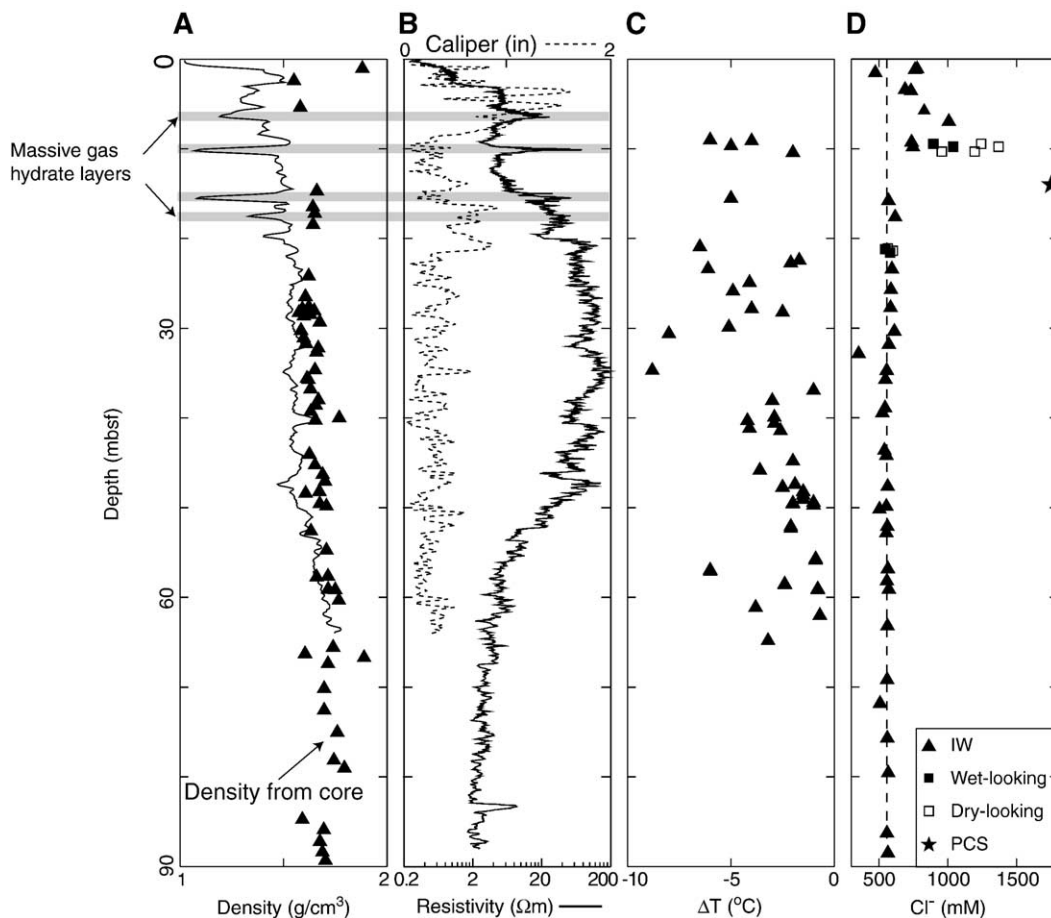


Fig. 6. Core and log data from ODP Site 1249. (A) LWD bulk density and MAD core density. (B) LWD deep resistivity (solid line) and caliper log (dashed line). (C) Negative temperature anomalies (measured immediately after core recovery). (D) Chloride concentrations. Standard whole-round samples (triangle) and selected wet- (closed square) and dry-looking (open square) samples are shown. The in situ salinity is also estimated from the Pressure Core Sampler (PCS; star). Dashed line indicates seawater salinity (550 mM Cl⁻).

Below 30 mbsf, logs reveal a 20-m-thick, high-resistivity zone with peak values exceeding $160 \Omega \text{ m}$ at 35 mbsf (Fig. 6B). Thermal anomalies and mousse-like textures resulting from hydrate dissociation are observed throughout this interval. Surprisingly, the PCS core recovered from 34 mbsf only contains hydrate of $\sim 5\%$ pore volume [28] (Fig. 7A). Core recovery improved significantly below 30 mbsf.

Pore fluids collected from the upper 20 mbsf at Site 1249 are enriched in Cl^- (Fig. 6D). Torres et al. [15] described how these interstitial water (IW) samples were obtained and showed that pore water chlorinity reaches 1008 mM at ~ 7 mbsf. Pairs of wet and adjacent dry sediment intervals were analyzed immediately after retrieval [15]. Pore fluids in the dry-looking samples have a Cl^- maximum of 1368 mM at ~ 10 mbsf. Milkov et al. [14] estimated in situ salinity and gas concentration through degassing a PCS core (~ 14 mbsf; star in Fig. 6D) and found that the in situ salinity ($\sim 1750 \text{ mM Cl}^-$) approximates the value required for three-phase equilibrium at that depth. Below 20 mbsf, high-chloride brines give way to the low-chloride anomalies.

3.2. ODP Site 1249: In situ salinity and water saturation

Pore waters collected from IW samples include both in situ salinity enrichment and a freshening component

due to hydrate dissociation during retrieval [12]. The in situ salinity may be calculated from a combination of electrical resistivity log, core-derived porosity and pore fluid salinity [29].

Archie's law describes the relation between formation resistivity (R_t) and water saturation (S_w):

$$S_w^n = \frac{aR_w}{\phi^m R_t}, \quad (3)$$

where n is the saturation exponent, a is the tortuosity coefficient and m is the cementation coefficient. The core-derived porosity ϕ is known from shipboard moisture and density measurements [12]. We derive a and m by cross-plotting LWD resistivity vs. core-derived porosity from Site 1250 below the BSR where there is no free gas (i.e., $S_w=1$) and pore fluid salinity is assumed to equal that of seawater. We find $a=3.65$ and $m=0.5$. These parameters are close to that derived from ODP Site 891 ($a=5.8$, $m=0.8$) [30]. At relatively low S_w , the water phase may form discrete drops within the pores [30] and n is relatively high. We take $n=1.9386$ [31] for Site 1250 and $n=4$ [30] for Site 1249. The latter value is high because Site 1249 is inferred to have low S_w .

We use an iterative method to estimate in situ salinity ($C_{\text{in situ}}$) and water saturation, because $C_{\text{in situ}}$ affects the resistivity. Pore-water resistivity (R_w) is calculated

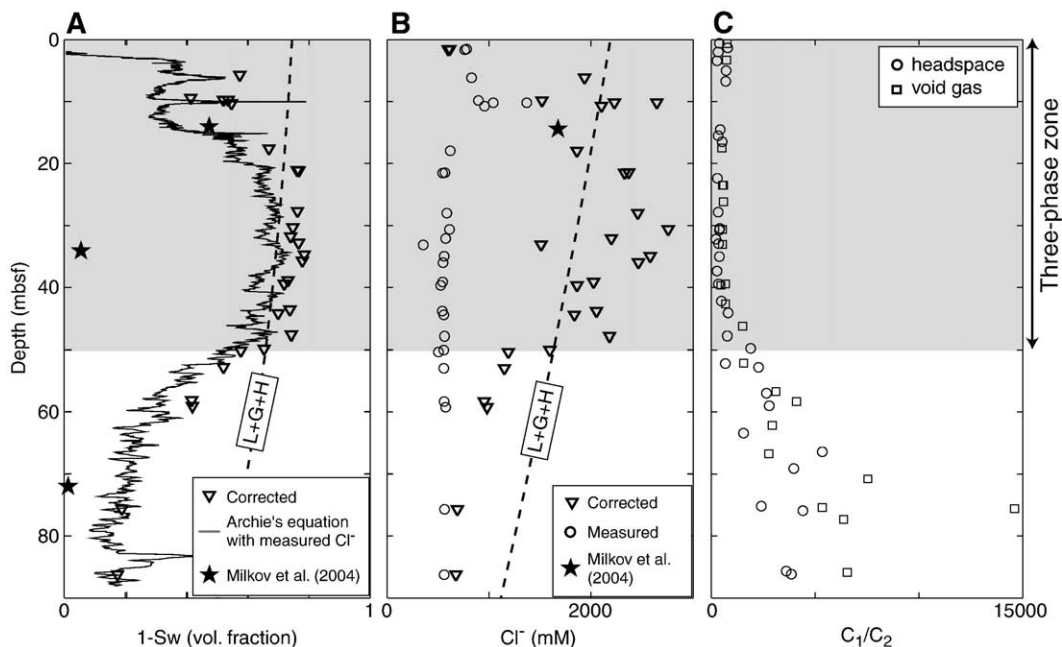


Fig. 7. Interpretation of ODP Site 1249. (A) $1 - S_w$ determined from the in situ salinity (triangle), the measured salinity (solid line) and the Pressure Core Sampler (PCS) measurement (star). (B) Measured (circle) vs. corrected (triangle) pore water salinity. Dashed line denotes salinity at three-phase equilibrium. Shaded area represents the three-phase zone. (C) C_1/C_2 ratio in gas void (square) and headspace (circle). Note that the BSR was not penetrated at this site.

as a function of temperature and salinity [32]. The core-measured salinity (C_{IW}) and its associated pore-water resistivity are initially input into Eq. (3) to obtain S_w . We assume that the dissociated hydrate produces an equal volume of freshwater; thus we use $C_{in\ situ} = C_{IW} / S_w$ to estimate the in situ salinity. Pore-water resistivity changes accordingly and S_w is recalculated. The iterative process is continued until the in situ salinity and water saturation do not change. The solution generally converges after a few iterations.

We calculate that $1 - S_w$ ranges from 20% to 80% at Site 1249 (triangle in Fig. 7A). $1 - S_w$ rapidly increases from the seafloor to 80% at 20 mbsf and there is a spike at 10 mbsf. Between 20 and 50 mbsf, $1 - S_w$ is $\sim 80\%$. Beneath 50 mbsf, $1 - S_w$ decreases to 20%. Compared to the iterative method, the standard Archie calculation with the measured salinity (solid line in Fig. 7A) [31] underestimates $1 - S_w$ by 5–10%.

The sediment pores must be filled with water, hydrate and/or free gas in situ. However, resistivity alone cannot distinguish the fraction of the pore space not filled with water ($1 - S_w$), because both free gas and hydrate have high resistivity [28]. Milkov et al. [14] indicated that the pore space at 14 mbsf from Site 1249 had 40% hydrate and 10% free gas. Schowalter [33] determined experimentally that 10% gas saturation is required for gas migration in shale. Our best estimate is that gas saturation is equal to or more than 10%; thus hydrate saturations are less than 70% at Site 1249.

The in situ salinity is much higher than that measured by pore-water squeezing (Fig. 7B). The zone between the seafloor and 50 mbsf has Cl^- concentrations of up to 2600 mM. In this zone, the in situ salinity gradually decreases with depth and the values are in general agreement with salinities inferred from a PCS

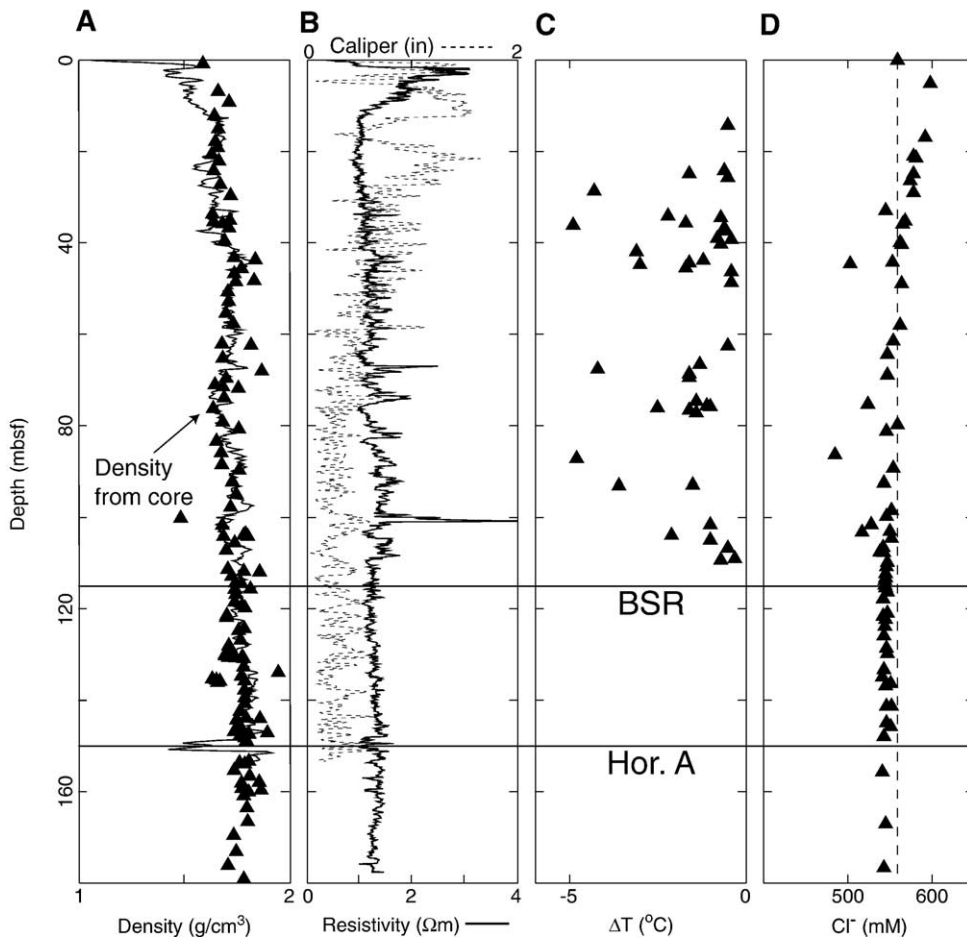


Fig. 8. Core and log data from ODP Site 1250. (A) LWD bulk density and MAD core density. (B) LWD deep resistivity (solid line) and caliper log (dashed line). (C) Negative temperature anomalies (measured immediately after core recovery). (D) Chloride concentrations. Standard whole-round samples (triangle) are shown. Dashed line indicates seawater salinity.

core (star in Fig. 7B) [14]. Below this zone, there is an abrupt downward decrease in salinity and in $1 - S_w$.

We interpret that three phases (gas, hydrate and water) coexist from the seafloor to 50 mbsf at Site 1249 (gray area in Fig. 7). In this zone, the in situ salinity falls near the three-phase equilibrium curve. However, beneath 50 mbsf, the in situ salinity is below the three-phase equilibrium curve and only two phases (hydrate and water) coexist.

3.3. ODP Site 1250: In situ salinity and water saturation

ODP Site 1250 was drilled 350 m southwest of ODP Site 1249 and 100 m east of the Pinnacle (Fig. 2). Site 1250 has a high-resistivity zone ($\sim 3 \Omega \text{ m}$) near the seafloor (Fig. 8B). Core recovery from this interval was poor. Below this interval, resistivity increases with depth and there are zones of high resistivity. Extensive cold anomalies are present (Fig. 8C), but poor core recovery limits detection of near-surface hydrate.

The pore fluids recovered from the upper 20 mbsf at Site 1250 also show Cl^- enrichment (Fig. 8D). However, the salinity enrichment is significantly lower than those measured at Site 1249. Cl^- reaches a maximum value of 613 mM at 13.9 mbsf. Below 30 mbsf, the Cl^- concentration is less than that of seawater. We use Eq. (3) to calculate $1 - S_w$ as described for Site 1249. At

Site 1250, hydrate is concentrated in a 10-m-thick zone just below the seafloor and the maximum $1 - S_w$ approaches 40% (Fig. 9A). Below this interval, hydrate is distributed over a broad depth range and $1 - S_w$ increases from approximately zero at 40 mbsf to 20% at the BSR (~ 114 mbsf).

The in situ salinity is lower at equivalent depths at Site 1250 than at Site 1249. The in situ salinity at Site 1250 only slightly exceeds the measured salinity (Fig. 9B), even in the near-surface hydrate zone. The in situ salinity falls below the three-phase equilibrium curve, indicating that only hydrate and water should coexist above the BSR at Site 1250.

4. Discussion

We have presented a model to describe how marine gas hydrate systems with abundant gas supply create local equilibrium conditions that allow free gas migration through the hydrate stability zone. Focused gas flow generates a local, moving, three-phase reaction front. The pore water salinity is buffered at the equilibrium value: hydrate forms until salinity increases to the point where free gas is stable and thereafter, gas migrates through the zone. The model provides a simple explanation for the presence of free gas within the RHSZ, does not rely on kinetics [15], and extends studies that suggest free gas is present within the RHSZ as a result of elevated salinity [14,15].

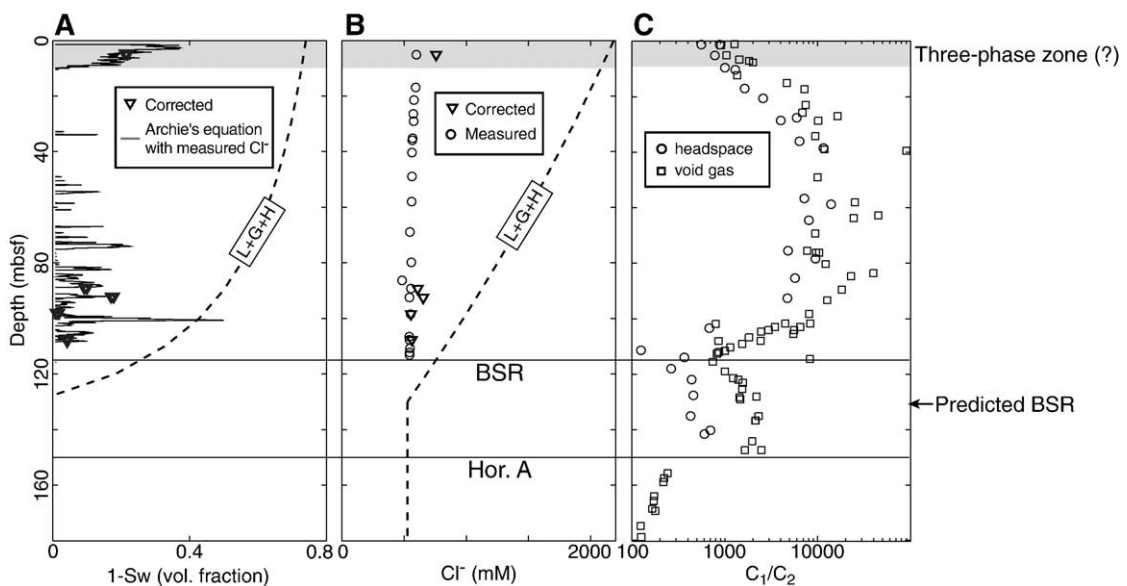


Fig. 9. Interpretation of ODP Site 1250. (A) $1 - S_w$ determined from the in situ salinity (triangle), the measured salinity (solid line). (B) Measured (circle) vs. corrected (triangle) pore water salinity. Dashed line denotes salinity at three-phase equilibrium. The in situ salinity is not sufficient for three-phase equilibrium. (C) C_1/C_2 ratio in gas void (square) and headspace (circle).

We document a zone of three-phase stability between the seafloor and 50 mbsf at ODP Site 1249 and suggest that there is a zone of three-phase stability from the BSR to the ridge crest where gas is venting today. The high salinity hypothesis is linked to observations of seismic wipeout zone located beneath the Pinnacle. Although southern Hydrate Ridge is a specific case, this model may apply to other settings where free gas migration within the hydrate stability zone has been inferred, such as the Gulf of Mexico [34], the Cascadia margin offshore Vancouver [19], the Caspian Sea [17] and the Blake Ridge [35,36].

4.1. Comparisons to other hydrate formation models

Previous hydrate formation models assumed that methane is transported only in the liquid phase by diffusion and slow advection [26,37–39]. This hydrate accumulation process is termed a flow-controlled gradient reaction [25]. These two-phase (hydrate and water+dissolved gas) models are only appropriate for low-methane flux regions. In these models, the change in solubility within the RHSZ is too small to generate a

significant hydrate amount and consequently no excess salinity is generated. Hydrate is concentrated at the base of the hydrate stability zone where the solubility gradient is greatest [26,37]. In contrast, we suggest that where methane flux is high, it is transported as a separate gas phase under buoyancy. Hydrate formation is limited by salt buildup and not by methane supply, free gas is present throughout the RHSZ, gas actively vents the surface and hydrate precipitates at or near the seafloor. In this model, salinity and hydrate saturation increase upward towards the seafloor.

4.2. Two-dimensional free gas migration at southern Hydrate Ridge

The model presented here is one-dimensional, with gas supplied from below. At southern Hydrate Ridge, the flow path is multi-dimensional (Fig. 10). Trehu et al. [40] suggested that beneath the BSR, gas is focused laterally along a high-permeability layer named Horizon A. Gas accumulated in Horizon A below the RHSZ until its high pressure forced gas to migrate upward into the RHSZ. The elevated gas pressure fractured the

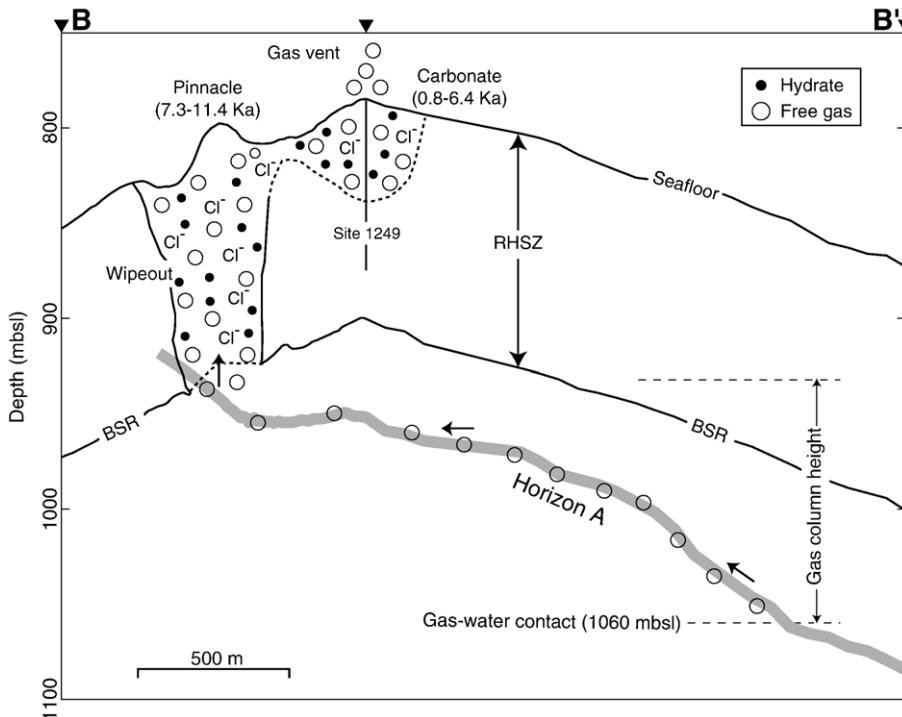


Fig. 10. Schematic diagram of the dynamic hydrate/free gas system at southern Hydrate Ridge (B–B' in Fig. 1). Free gas migrates up the conduit (i.e., Horizon A) under a strong buoyancy force and first become hydrated where Horizon A crosses the RHSZ. Gas is trapped beneath this hydrate seal until the pressure at the top of the gas column is high enough to drive gas into the RHSZ. High gas flux from Horizon A initiates rapid hydrate formation and pore water salinity is increased to the point where free gas will locally be thermodynamically stable. The massive, near-surface carbonate deposits form an impermeable barrier. As a result, the gas rising from depth is laterally diverted to the crest.

hydrate-bearing sediments and transported gas upward through the hydrate layer. We suggest that gas migrated vertically below the Pinnacle. The BSR was disrupted and the low-amplitude chimney was caused by upward migration of free gas (Fig. 2). Subsequently, gas flow was diverted laterally by near-surface low-permeability carbonate layers to the ridge summit where gas is actively venting at present (Fig. 10) [10].

Sediments at southern Hydrate Ridge contain mainly microbial C_1 but C_{2+} hydrocarbon gases of thermogenic origin are also present. The three-phase zones are enriched in C_2 . At Site 1249, the C_1/C_2 ratio is constant (<1000) in the three-phase stability zone (0–50 mbsf) and then abruptly increases down to the base of the cored section (~ 5000) (Fig. 7C). The near-surface hydrate zone (0–10 mbsf) at Site 1250 also has low C_1/C_2 ratios (Fig. 9C). Horizon A penetrated at Site 1250 also reveals C_2 enrichment (Fig. 9C) and the C_1/C_2 ratios are similar to those in the three-phase zone at Sites 1249 and 1250. We interpret that C_{2+} hydrocarbon gases are supplied to the base of the RHSZ from the deeper permeable Horizon A (Fig. 10) and that zones of C_2 enrichment represent the gas migration pathway.

Steady gas venting requires three-phase equilibrium along the entire migration path. Although Site 1250 lies between the Pinnacle and the summit (Fig. 2), the in situ salinity is not sufficient to stabilize free gas (Fig. 9B). We suggest that the three-phase zone may exist in the upper 10 mbsf at Site 1250 for three reasons. First, borehole conditions were especially degraded near the top (Fig. 8B), resulting in large-scale, negative shifts in the electrical resistivity log. Second, the sulfate–methane interface is very near the seafloor [12], typical of the influence of free gas. Third, the near-surface zone at Site 1250 (Fig. 9C) has anomalously low C_1/C_2 ratio similar to the three-phase zone at Site 1249 (Fig. 7C).

Southern Hydrate Ridge may have evolved from an early phase where methane-rich water vented to the present-day phase where gas is venting. During early gas accumulation, methane-rich water was vertically displaced from Horizon A to the seafloor and this aqueous flow may have formed the Pinnacle. Later, sufficient gas entered the hydrate stability zone to create a gas pathway to the Pinnacle. However, low permeability at the Pinnacle drove flow laterally resulting in venting at the summit. However, massive authigenic carbonates are not present at the summit [7], suggesting that focused gas venting has recently begun here. The evolution from methane-rich water to gas venting is consistent with variations in the age of the authigenic carbonates from the Pinnacle (7.3–11.4 Ka) to the summit (0.8–6.4 Ka) (Fig. 10) [41].

4.3. Scaling arguments

The gas flux out of the crest of southern Hydrate Ridge is estimated to be $\sim 10^2$ mol CH_4 m^{-2} yr^{-1} [15]. This corresponds to a gas Darcy velocity of $\sim 10^{-9}$ m s^{-1} , assuming a gas density of 62.8 kg m^{-3} [40]. The equilibration length (l_e) is only $\sim 10^{-6}$ m (Eq. (2)), much smaller than the thickness of the hydrate stability zone. Thus, the assumption of local thermodynamic equilibrium is valid. In the Appendix, we calculate that gas depletion rate caused by loss of salt (<10 mol CH_4 m^{-2} yr^{-1}) is far less than gas supply rate ($\sim 10^2$ mol CH_4 m^{-2} yr^{-1}); thus the assumption of no large-scale diffusion is appropriate.

The model assumes a constant temperature gradient. Heat advection by the gas flow and the heat released by crystallization of hydrate could perturb this constant gradient. The thickness of the RHSZ (Δz) is 120 m, the gas flux (q_g) is 10^2 mol CH_4 m^{-2} yr^{-1} [15], the thermal conductivity (K) is ~ 1.0 $\text{W m}^{-1} \text{ }^\circ\text{C}^{-1}$ [12] and the gas heat capacity (c_g) is 3.5 $\text{kJ kg}^{-1} \text{ }^\circ\text{C}^{-1}$ [23]. In this case the Peclet number ($Pe = q_g c_g \Delta z / K$) is ~ 0.02 and thus advection of heat can be neglected [42]. If the latent heat of crystallization of hydrate (L) is 42.1 kJ kg^{-1} [42] and the normal heat flow at southern Hydrate Ridge is ~ 55 mW m^{-2} (the thermal conductivity is ~ 1.0 $\text{W m}^{-1} \text{ }^\circ\text{C}^{-1}$ [12] and the geothermal gradient is 55 $^\circ\text{C km}^{-1}$ [15]), the heat added by hydrate formation at the reaction front ($q_e = 7.5 q_g L$) is $16 \sim 20$ mW m^{-2} , which is a significant fraction of the normal heat flow. Thus the latent heat of hydrate formation may cause significant derivation from the linear thermal gradient in a one-dimensional model.

However, we interpret that a large fraction of the released latent heat will be dissipated laterally from the gas chimney. We estimate that it takes ~ 30 yrs to fill a sediment volume (1 m thickness and 150 m half-width) at 50 mbsf with hydrates ($\sim 65\%$ of pore volume). Upon formation, this amount of hydrate laterally releases $\sim 10^6$ kJ of heat to the surrounding. If the heat capacity per unit volume of sediment is 2.3 $\text{J cm}^{-3} \text{ }^\circ\text{C}^{-1}$ [42] and the thermal diffusivity is 10^{-6} $\text{m}^2 \text{ s}^{-1}$ [36], the positive thermal anomaly of the gas chimney decays to less than 1 $^\circ\text{C}$ in 30 yrs according to Turcotte and Schubert [43].

The model assumes a hydrostatic pressure gradient and no water flow. However, the volume change of hydrate formation produces a divergence of flow. However, the associated flow is very small since methane hydrate density is only $\sim 8\%$ lower than water density [1]. Variations in salinity and water density across the hydrate zone may generate a density-driven convection

below the seafloor. We assume the water viscosity (μ_w) is 10^{-3} Pa s, the chemical diffusivity (D) is 10^{-9} m² s⁻¹ [36], the permeability (k) is 10^{-16} m² [27], the thickness of the RHSZ (Δz) is 120 m, and the water density difference between the seafloor and the base of the RHSZ ($\Delta\rho_w$) is 75 kg m⁻³. The Rayleigh number ($Ra = \Delta\rho_w k \Delta z / \mu_w D$) is only ~ 0.9 , which is not sufficient to initiate a convection [43].

We assume no basal water flux at southern Hydrate Ridge. This assumption is justified by estimating fluid mobility. Fluid mobility is proportional to relative permeability and inversely proportional to viscosity [40]. The gas viscosity is much lower than the water viscosity, and the gas relative permeability is much higher than the water relative permeability because of the very high gas saturation (up to 90%) in Horizon A [40]. Thus the flux of gas out of Horizon A will greatly exceed the flux of water.

4.4. Implications for hydrate reservoir stability

We propose that there is a direct pathway for free gas migration from the free gas zone beneath the RHSZ to the seafloor and that this migration pathway forms very rapidly. As a result, significant amounts of gaseous methane can bypass the RHSZ without forming hydrate. Thus, in areas where gas flow is focused, such as Hydrate Ridge, significant amounts of free gas may enter the ocean without forming hydrate, which changes the expected behaviors of the hydrate capacitor [5]. In addition, hydrate at three-phase equilibrium is more susceptible to environmental changes than hydrate that forms in the two-phase region. In our model, all the hydrates are already at the three-phase boundary, so they would respond easily and rapidly to bottom-water warming or sea-level lowering during climate change.

We estimate that at southern Hydrate Ridge, bottom-water warming from 4 to 8 °C can release $\sim 70\%$ of methane stored in hydrates, which are initially at three-phase equilibrium. During warming, hydrate dissociation releases fresh water and decreases salinity until the undissociated hydrates are brought back into equilibrium with venting gas at the new temperature. The new three-phase zone becomes thinner, fresher, and less hydrate-enriched. Hydrates in the region between the initial and the new three-phase stability zone will dissociate into gas and fresh water. Since the hydrate zone is always buffered at three-phase equilibrium, then dissociated gas will be quickly released to the ocean rather than recrystallize as hydrates at shallow depths.

5. Conclusions

Free methane gas is venting through the regional hydrate stability zone (RHSZ) at southern Hydrate Ridge. Free gas supplied from below forms hydrate, depletes water and elevates salinity until pore water is too saline for further hydrate formation. This system self-generates local three-phase equilibrium and allows free gas migration to the seafloor. Log and core data document a zone of three-phase stability between the seafloor and 50 mbsf at ODP Site 1249. We suggest that there is a zone of three-phase stability from the disrupted BSR to the ridge crest where gas is venting today. This process provides a mechanism for gas venting through the hydrate stability zone that is observed around the world. In these settings, the RHSZ is no longer a thermodynamic barrier to free gas migration.

Nomenclature

g	Free gas phase
h	Hydrate phase
l	Liquid phase
m	Methane
w	Water
Δz	Thickness of RHSZ (L)
ϕ	Porosity (dimensionless)
ρ_h	Hydrate density (M L ⁻³)
ρ_w	Water density (M L ⁻³)
μ_w	Water viscosity (M L ⁻¹ T ⁻¹)
a	Tortuosity coefficient (dimensionless)
b	Half-width of chimney (L)
c_g	Gas heat capacity (L ² T ⁻² Θ^{-1})
f	Fugacity (M L ⁻¹ T ⁻²)
k	Permeability (L ²)
l_e	Equilibration length (L)
m	Cementation coefficient (dimensionless)
n	Saturation exponent (dimensionless)
q_e	Heat flux (M T ⁻³)
q_g	Gas flux (M L ⁻² T ⁻¹)
z	Depth below seafloor (L)
C	Salinity (dimensionless)
D	Chemical diffusivity (L ² T ⁻¹)
F	Formation factor (dimensionless)
K	Thermal conductivity (M L T ⁻³ Θ^{-1})
L	Latent heat (L ² T ⁻²)
P	Pressure (M L ⁻¹ T ⁻²)
R_w	Formation water resistivity (M L ³ T ⁻² A ⁻²)
R_t	Formation resistivity (M L ³ T ⁻² A ⁻²)
S_g	Gas saturation (dimensionless)
S_h	Hydrate saturation (dimensionless)
S_w	Water saturation (dimensionless)
T	Temperature (Θ)

Acknowledgements

This research used data provided by the Ocean Drilling Program (ODP). ODP is sponsored by the US National Science Foundation (NSF) and participating countries under management of Joint Oceanographic Institutions (JOI), Inc. The manuscript benefited from the critical review and insightful comments of Wenyue Xu, Demian Saffer, Matra Torres, Anne Trehu, Derek Elsworth, Luis Ayala and an anonymous reviewer. Funding for research was provided by the Penn State Geofluids Consortium and a JOI/USSAC Fellowship (Liu).

Appendix A. Half-space salt diffusion with gas supply from depth

Consider a vertical zone of elevated salinity through which gas is being transported within the RHSZ. At depth z , the gas chimney is kept at three-phase equilibrium salinity $C_{\text{eq}}(z)$ and initially the bounding pore water has normal salinity C_{sw} .

The total amount of salt lost from the chimney to the bounding pore water is given by (mass per unit area) [43]

$$2\phi\rho_w[C_{\text{eq}}(z) - C_{\text{sw}}]\sqrt{\frac{Dt}{\pi}}, \quad (\text{A.1})$$

where D is the chemical diffusivity for Cl^- . Equilibrium requires further growth of the hydrate to compensate the loss of salt by lateral diffusion. The chimney is maintained at three-phase equilibrium by further hydrate formation. If S_h increases by ΔS_h over a time interval t , S_w decreases by ΔS_h accordingly. Note that S_w and S_h refer to the volume fractions of water and hydrate in the original space and that free gas expands the volume when it becomes stable. Thus, the amount of salt in the chimney decreases by (mass per unit area)

$$\phi\rho_w b C_{\text{eq}}(z) \Delta S_h(z, t), \quad (\text{A.2})$$

where b is the half-width of the chimney. This provides a minimum estimate of the change in S_w . Following mass conservation for salt, the decrease in the amount of salt in the chimney equals that lost to the bounding pore water. By equating (A.1) and (A.2), we obtain

$$\phi\rho_w b C_{\text{eq}}(z) \Delta S_h(z, t) = 2\phi\rho_w [C_{\text{eq}}(z) - C_{\text{sw}}] \sqrt{\frac{Dt}{\pi}}. \quad (\text{A.3})$$

Over this time interval, the S_h increase needed to maintain the equilibrium is

$$\Delta S_h(z, t) = \frac{2}{b} \left(1 - \frac{C_{\text{sw}}}{C_{\text{eq}}(z)}\right) \sqrt{\frac{Dt}{\pi}}. \quad (\text{A.4})$$

The rate of CH_4 depletion (mass per unit volume per unit time) as a result of loss of salt is given by

$$q_{\text{sink}}(z, t) = \frac{M_{\text{CH}_4}}{M_h} \rho_h \frac{\partial \Delta S_h(z, t)}{\partial t}, \quad (\text{A.5})$$

where M_{CH_4} and M_h are the molecular weights of methane and hydrate respectively. Substituting (A.4) into (A.5) yields

$$q_{\text{sink}}(z, t) = \frac{M_{\text{CH}_4}}{M_h} \frac{\rho_h}{b} \left(1 - \frac{C_{\text{sw}}}{C_{\text{eq}}(z)}\right) \sqrt{\frac{D}{\pi t}}. \quad (\text{A.6})$$

Integrating q_{sink} along the chimney with height Z , we obtain the total rate of CH_4 depletion (mass per unit area per unit time) due to loss of salt

$$Q_{\text{sink}}(t) = \int_0^Z q_{\text{sink}}(z, t) dz. \quad (\text{A.7})$$

The gas supply rate from depth is denoted by Q_{source} (mass per unit area per unit time). If $Q_{\text{source}} > Q_{\text{sink}}$, free gas is rapidly supplied into the chimney relative to the rate at which the excluded salt laterally diffuses. Gas supply is sufficient to maintain the chimney at three-phase equilibrium. If $Q_{\text{source}} < Q_{\text{sink}}$, diffusion of salt is significant compared with gas supply and three-phase equilibrium cannot be maintained.

At southern Hydrate Ridge, we assume the gas chimney has a porosity of 0.6, a height of 120 m and a half-width of 150 m (Fig. 10). Based on dating of the vent carbonates [41], the gas chimney extended to the ridge crest at ~ 7 Ka BP. Given the chemical diffusivity $D = 10^{-9} \text{ m}^2 \text{ s}^{-1}$ [36], gas supply ($\sim 10^2 \text{ mol CH}_4 \text{ m}^{-2} \text{ yr}^{-1}$) is more rapid than gas depletion ($< 10 \text{ mol CH}_4 \text{ m}^{-2} \text{ yr}^{-1}$) caused by loss of salt. Thus, it is reasonable to assume no large-scale diffusion.

References

- [1] E.D. Sloan, Clathrate Hydrates of Natural Gases, Marcel Dekker, New York, 1998, 705 pp.
- [2] K.A. Kvenvolden, Gas hydrates: geological perspective and global change, Rev. Geophys. 31 (1993) 173–187.
- [3] R.D. Hyndman, E.E. Davis, A mechanism for the formation of methane hydrate and seafloor bottom-simulating reflectors by vertical fluid expulsion, J. Geophys. Res. 97 (1992) 7025–7041.
- [4] A.V. Milkov, R. Sassen, Economic geology of offshore gas hydrate accumulations and provinces, Mar. Pet. Geol. 19 (2002) 1–11.
- [5] G.R. Dickens, Rethinking the global carbon cycle with a large, dynamic and microbially mediated gas hydrate capacitor, Earth Planet. Sci. Lett. 213 (2003) 169–183.

- [6] R.E. Kayen, H.J. Lee, Pleistocene slope instability of gas hydrate-laden sediment on the Beaufort Sea margin, *Mar. Geotechnol.* 10 (1991) 125–141.
- [7] A.M. Trehu, G. Bohrmann, M.E. Torres, G.F. Moore, E. Suess, Temporal and spatial evolution of a gas hydrate-bearing accretionary ridge on the Oregon continental margin, *Geology* 27 (1999) 939–942.
- [8] N.L. Bangs, D.S. Sawyer, X. Golovchenko, Free gas at the base of the gas hydrate zone in the vicinity of the Chile triple junction, *Geology* 21 (1993) 905–908.
- [9] W.S. Holbrook, D. Lizarralde, H. Hoskins, W.T. Wood, R.A. Stephen, Methane hydrate and free gas on the Blake Ridge from vertical seismic profiling, *Science* 273 (1996) 1840–1843.
- [10] K.U. Heeschen, A.M. Trehu, R.W. Collier, E. Suess, G. Rehder, Distribution and height of methane bubble plumes on the Cascadia Margin characterized by acoustic imaging, *Geophys. Res. Lett.* 30 (2002) 1–4.
- [11] E. Suess, R.W. Collier, J. Greinert, P. Linke, G. Rehder, A. Trehu, K. Wallmann, G. Winckler, E. Zuleger, M.E. Torres, G. Bohrmann, Gas hydrate destabilization: enhanced dewatering, benthic material turnover and large methane plumes at the Cascadia convergent margin, *Earth Planet. Sci. Lett.* 170 (1999) 1–15.
- [12] A.M. Trehu, G. Bohrmann, F.R. Rack, M.E. Torres, et al., *Proc. ODP Init. Repts.* 204 (2003).
- [13] F. Abegg, J. Freitag, G. Bohrmann, W. Brueckmann, A. Eisenhauer, H. Aman, H.-J. Hohnberg, Free Gas Bubbles in the Hydrate Stability Zone: Evidence from CT Investigation under In Situ Conditions, Spring 2003, abstract #EAE-A-10342, AGU meeting, Nice, France.
- [14] A.V. Milkov, Y.-J. Lee, W.S. Borowski, M.E. Torres, W. Xu, H. Tomaru, A.M. Trehu, P. Schultheiss, G.R. Dickens, G.E. Claypool, Co-existence of gas hydrate, free gas, and brine within the regional gas hydrate stability zone at Hydrate Ridge (Oregon margin): evidence from prolonged degassing of a pressurized core, *Earth Planet. Sci. Lett.* 222 (2004) 829–843.
- [15] M.E. Torres, K. Wallmann, A.M. Trehu, G. Bohrmann, W.S. Borowski, H. Tomaru, Gas hydrate growth, methane transport, and chloride enrichment at the southern summit of Hydrate Ridge, Cascadia margin off Oregon, *Earth Planet. Sci. Lett.* 226 (2004) 225–241.
- [16] M. Haeckel, E. Suess, K. Wallmann, D. Rickert, Rising methane gas bubbles form massive hydrate layers at the seafloor, *Geochim. Cosmochim. Acta* 68 (2004) 4335–4345.
- [17] G.D. Ginsburg, V.A. Soloviev, Methane migration within submarine gas-hydrate stability zone under deep-water conditions, *Mar. Geol.* 137 (1997) 49–57.
- [18] M.B. Clennell, W.J. Winters, M. Hovland, J.S. Booth, P. Henry, Formation of natural gas hydrates in marine sediments 1. Conceptual model of gas hydrate growth conditioned by host sediment properties, *J. Geophys. Res.* 104 (1999) 22985–23003.
- [19] W.T. Wood, R.D. Hyndman, J.F. Gettrust, N.R. Chapman, G.D. Spence, Decreased stability of methane hydrates in marine sediments owing to phase-boundary roughness, *Nature* 420 (2002) 656–660.
- [20] P. Henry, M. Thomas, M.B. Clennell, Formation of natural gas hydrates in marine sediments 2. Thermodynamic calculations of stability conditions in porous sediments, *J. Geophys. Res.* 104 (1999) 23005–23022.
- [21] Z.H. Duan, N. Moller, J. Greenberg, J.H. Weare, The prediction of methane solubility in natural waters to high ionic strength from 0 to 250 C and from 0 to 1600 bar, *Geochim. Cosmochim. Acta* 56 (1992) 1451–1460.
- [22] R. Hesse, W. Harrison, Gas hydrate (clathrate) causing pore water freshening and oxygen isotope fractionation in deep-water sedimentary sections of terrigenous continental margins, *Earth Planet. Sci. Lett.* 55 (1981) 55453–55462.
- [23] W. Xu, Phase balance and dynamic equilibrium during formation and dissociation of methane gas hydrate, *Proc. of the 4th International Conference on Gas Hydrates, Yokohama, 2002*, pp. 195–200.
- [24] W. Xu, Modeling dynamic marine gas hydrate systems, *Am. Min.* 89 (2004) 1271–1279.
- [25] O.M. Phillips, *Flow and Reactions in Permeable Rocks*, Cambridge, New York, 1991, 285 pp.
- [26] A.W. Rempel, B.A. Buffett, Formation and accumulation of gas hydrate in porous media, *J. Geophys. Res.* 102 (1997) 10151–10164.
- [27] B. Tan, J.T. Germaine, P.B. Flemings, Consolidation and strength characteristics of sediments from ODP Site 1244, Hydrate Ridge, Cascadia Continental Margin, *Proc. ODP Sci. Results* 204 (submitted for publication).
- [28] A.M. Trehu, P.E. Long, M.E. Torres, G. Bohrmann, F.R. Rack, et al., Three-dimensional distribution of gas hydrate beneath southern Hydrate Ridge: constraints from ODP Leg 204, *Earth Planet. Sci. Lett.* 222 (2004) 845–862.
- [29] R.D. Hyndman, T. Yuan, K. Moran, The concentration of deep sea gas hydrates from downhole electrical resistivity logs and laboratory data, *Earth Planet. Sci. Lett.* 172 (1999) 167–177.
- [30] E. Spangenberg, Modeling of the influence of gas hydrate content on the electrical properties of porous sediments, *J. Geophys. Res.* 106 (2001) 6535–6548.
- [31] T.S. Collett, J. Ladd, Detection of gas hydrate with downhole logs and assessment of gas hydrate concentrations (saturations) and gas volumes on the Blake Ridge with electrical resistivity log data, *Proc. ODP Sci. Results* 164 (2000) 179–191.
- [32] Schlumberger, *Log Interpretation Principles/Applications*, Schlumberger, Houston, 1989, 208 pp.
- [33] T.T. Schowalter, Mechanics of secondary hydrocarbon migration trapping, *Am. Assoc. Pet. Geol. Bull.* 63 (1979) 723–760.
- [34] I.R. Macdonald, L. Lee, K.T. Scott, N.L. Guinasso, R. Sassen, J.M. Brooks, Gas hydrate that breaches the sea floor on the continental slope of the Gulf of Mexico, *Geology* 22 (1994) 699–702.
- [35] C.K. Paull, W. Ussler, W.S. Borowski, F.N. Spiess, Methane-rich plumes on the Carolina continental rise: associations with gas hydrates, *Geology* 23 (1995) 83–84.
- [36] M.H. Taylor, W.P. Dillon, I.A. Pecher, Trapping and migration of methane associated with the gas hydrate stability zone at the Blake Ridge Diapir, *Mar. Geol.* 164 (2000) 79–89.
- [37] W. Xu, C. Ruppel, Predicting the occurrence, distribution, and evolution of methane gas hydrate in porous marine sediments, *J. Geophys. Res.* 104 (1999) 5081–5095.
- [38] M.K. Davie, B.A. Buffett, A numerical model for the formation of gas hydrate below the seafloor, *J. Geophys. Res.* 106 (2001) 497–514.
- [39] M.K. Davie, B.A. Buffett, A steady state model for marine hydrate formation: constraints on methane supply from pore water sulfate profile, *J. Geophys. Res.* 108 (2003), doi:10.1029/2002JB002300.
- [40] A.M. Trehu, P.B. Flemings, N.L. Bangs, J. Chevallier, E. Gracia, J.E. Johnson, C.-S. Liu, X. Liu, M. Riedel, M.E. Torres, Feeding

- methane vents and gas hydrate deposits at south Hydrate Ridge, *Geophys. Res. Lett.* 31 (2004), doi:10.1029/2004GL021286.
- [41] B.M.A. Teichert, B. Bock, P. Linke, A. Eisenhauer, G. Bohrmann, A. Haase-Schramm, U/Th systematics and ages of authigenic carbonates from Hydrate Ridge, Cascadia Margin: recorders of fluid flow variations, *Geochim. Cosmochim. Acta* 67 (2003) 3845–3857.
- [42] L.M. Cathles, D.F. Chen, A compositional kinetic model of hydrate crystallization and dissolution, *J. Geophys. Res.* 109 (2004), doi:10.1029/2003JB002910.
- [43] D.L. Turcotte, G. Schubert, *Geodynamics*, Cambridge University Press, Cambridge, 2002, 456 pp.